

Understanding the hydrocarbon – PFSA ionomer conductivity gap in hydrogen fuel cells

Article

Accepted Version

Bangay, W., Yandrasits, M. and Hayes, W. ORCID:
<https://orcid.org/0000-0003-0047-2991> (2025) Understanding
the hydrocarbon – PFSA ionomer conductivity gap in hydrogen
fuel cells. *Physical Chemistry Chemical Physics*, 27 (16). pp.
8305-8319. ISSN 1463-9076 doi: 10.1039/d5cp00334b
Available at <https://centaur.reading.ac.uk/122805/>

It is advisable to refer to the publisher's version if you intend to cite from the work. See [Guidance on citing](#).

To link to this article DOI: <http://dx.doi.org/10.1039/d5cp00334b>

Publisher: Royal Society of Chemistry

All outputs in CentAUR are protected by Intellectual Property Rights law, including copyright law. Copyright and IPR is retained by the creators or other copyright holders. Terms and conditions for use of this material are defined in the [End User Agreement](#).

www.reading.ac.uk/centaur

CentAUR

Central Archive at the University of Reading

Reading's research outputs online

Cite this: DOI: 00.0000/xxxxxxxxxx

Understanding the hydrocarbon - PFSA ionomer conductivity gap in hydrogen fuel cells

William Bangay,^{*ab} Michael Yandrasits,^a and Wayne Hayes^b

Received Date

Accepted Date

DOI: 00.0000/xxxxxxxxxx

Hydrocarbon ionomers (HCs) have the potential to replace perfluorinated sulfonic acids (PFSAs), which are currently used in electrolyser or fuel cell membranes. To be a truly viable alternative, HCs must have conductivity across the operating range and cell lifetime comparable to PFSAs. Conductivity is an important property of membranes because it affects the energy efficiency of a fuel cell or electrolyser. By examining conductivity as a function of water volume fraction, it becomes evident that HC ionomers have consistently lower conductivity at low relative humidity. To better understand this 'conductivity gap', conductivity was converted to proton diffusivity and analysed using General Effective Media (GEM) theory for the first time. This analysis revealed that all ionomers require similar hydration levels for proton dissociation, and proton diffusion coefficients in the dry polymer are responsible for the conductivity gap. It is suggested that the membrane tortuosity ultimately accounts for the dry membrane's proton diffusivity and low RH conductivity. As the membrane hydrates however, all ionomers exhibit similar diffusion coefficients, indicating that conductivity at high humidity is limited by proton concentration.

1 Introduction

Fuel cell (FC) and water electrolyser (WE) membranes based on proton conducting ionomers are being commercialised because of their performance, durability, and electrical insulation properties. The most widespread ionomers in commercial use are perfluorosulfonic acid (PFSA) ionomers which combine chemical durability with high conductivity across the operational range of fuel cells and electrolysers. However, PFSA ionomers are classified as a "per- and polyfluoroalkyl substances" (PFAS), a group of chemicals which accumulate in the environment and do not biodegrade, granting them the "forever chemical" epithet.¹ The growing concern surrounding the use of PFAS materials has renewed interest in fluorine-free alternatives.

Promising alternatives are hydrocarbon ionomers (HC) which, like PFSA ionomers, utilise sulfonic acids as the proton donating moieties.²⁻⁴ HC ionomers are typically based on aromatic backbones although a few examples of aliphatic backbones have been reported.⁵ Critically, both do not contain PFAS groups, making them potential alternatives to PFSA ionomers. However, for HC ionomers to become economically viable alternatives to PFSAs, they must demonstrate superior properties (*e.g.* conductivity, durability, lifetime) beyond simply being a fluorine-free material.

Once a HC ionomer is processed into a membrane, one of the key comparatives is conductivity which quantifies the ease of proton transfer across a membrane. Membranes with high conductivity require lower voltage to drive a current which improves the energy conversion efficiency of the electrochemical system.

This analysis uses PFSA ionomers as the industrially set benchmark, enabling a clear comparison for different HC ionomers. Fig.1 plots the published conductivity of different ionomers across the operational humidity range. Despite the scattered data, fitted trend lines show the behavioural differences between the materials. At high relative humidity (RH) (*i.e.* RH greater than 60%) PFSA and HC datasets essentially overlap. Larger separation between datasets is observed at lower RH, with HC ionomers exhibiting lower conductivity than PFSA ionomers. The claim that HC ionomer conductivity is inferior at low relative humidity is not new, having been described in previous publications.⁵⁻¹⁰ This analysis labels the conductivity difference at low RH as the "conductivity gap". Bridging this gap is necessary if a fluorine-free alternative is to be economically viable, considering fuel cell system designers will otherwise choose the more conductive PFSA ionomer to maximize energy efficiency.

Examining results like those seen in Fig. 1 raises a fundamental question: what makes HC ionomer conductivity lower than that of a PFSA ionomer? Being a broad question, it is best to break it down into smaller components and investigate the various aspects on a case by case basis. The points explored are the role of proton concentration on conductivity, how acidity impacts the proton concentration, and the nuances of proton diffusion.

^a Johnson Matthey Technology Centre, Sonning Common, Reading, UK. E-mail: william.bangay@matthey.com

^b University of Reading, Reading, UK.

† Supplementary Information available: [details of any supplementary information available should be included here]. See DOI: 10.1039/cXCP00000x/

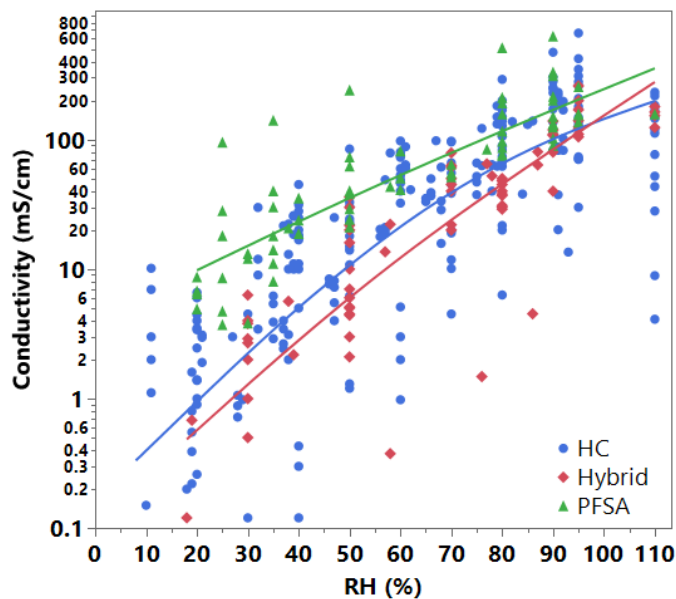


Fig. 1 Conductivity at 80 °C against relative humidity, data at 110% RH represents submerged conductivity measured in water. Marker color and shape represent the polymer type, with spline curves to illustrate trends. Data taken from references 5,7–31. Ionomers labelled 'Hybrid' are neither PFSA nor HC, as the ionomer contains fluorine but not the moieties characteristic of a PFSA. An alternative version of this figure which separates data into three acid concentration (see section 3.5) is available in Fig. S1 of the ESI.†

To support any claims a large dataset is required. As such, this analysis uses conductivity and water uptake data from 21 publications issued between 2006 and 2023, totalling 393 data points that represent 16 broad polymer categories.

The role of the diffusion coefficient on conductivity is found to be the most complex and significant. This is attributed to the percolation of a water network within the membrane, as described by the fitting parameters of the General Effective Medium (GEM) theory. These parameters are then linked to various polymeric attributes, providing insight into how polymer characteristics influence diffusion behaviour. Finally, case studies are used to better understand the HC-PFSA conductivity gap and to suggest potential strategies for closing it.

2 Dataset

The dataset used for this study was collected from publications which included both water uptake (WU) and conductivity data measured under the same conditions (*i.e.* temperature and humidity/submerged). Conductivity and WU were both required for the analysis discussed in this publication. This condition restricted the number of potential publications that could be analysed. The software WebPlotDigitizer was used to collect the published data as accurately as possible.³² Alongside the conductivity and WU data, the following metadata were stored; ion exchange capacity (IEC), measurement temperature, dry polymer density, polymer type, sulfonic acid type (*i.e.* hydrocarbon or fluorocarbon), polymer family, and, for block polymers, the ratio of hydrophilic to hydrophobic blocks.

All conductivity data was ex-situ, in-plane resistance measure-

ments either by direct current or alternating current. This membrane resistance was then converted to conductivity using the dry membrane dimensions. Conductivity determination using dry dimensions is different from the true conductivity which should consider the swollen dimensions from when the resistance value was measured. Without knowing the true width, length, and height of the sample when the resistance was measured this cannot be accounted for and dry dimensions are assumed. This is an uncertainty for conductivity values collected in literature and, by extension, the diffusion coefficients calculated within this analysis. This uncertainty is larger as the membrane swells more due to the greater difference between dry and swollen dimensions. A plot illustrating the difference between dry *versus* swollen dimension conductivity can be found in Fig. S2 of the ESI.†

Since temperature has a significant impact on conductivity, the collected dataset was filtered to 80 °C data only. This was the most common and most industrially applicable temperature (see Fig. S3 in ESI for data count against temperature).† An overview of the accrued data is provided in Fig. 2, showing the broad range of polymers analysed. (Note that 'Hybrid' was the name selected to represent polymers which lack the key structural elements of a PFSA material, but contain F and thus are not solely HC. Consequently, this study treats Hybrid materials as an entirely separate group).

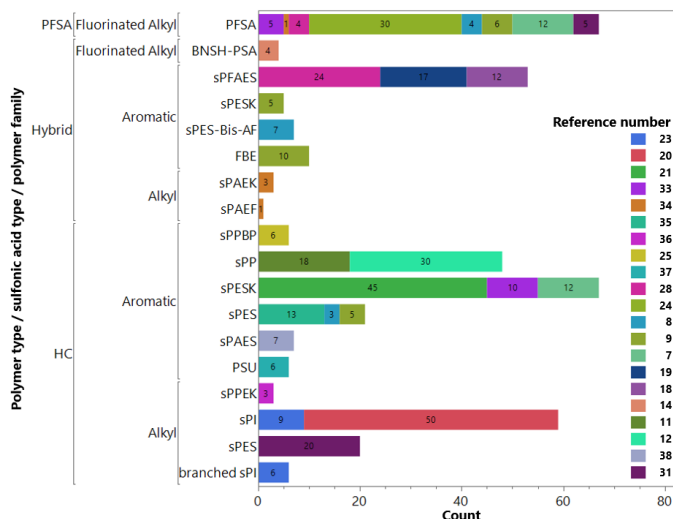


Fig. 2 Overview of collected data points (total 401), separated by the following sequential order, polymer type, sulfonic acid type, polymer family. Data colour represents the data source, data taken from 7–9,11,12,14,18–21,23–25,28,31,33–38

To accurately determine the goodness of fit, the number of fitting points must exceed the number of fitting parameters within a given model. The GEM model used to examine water network percolation uses 4 fitting parameters, and so the dataset was filtered to remove all polymers with less than 5 data points.^{39,40} This 'pruning' left 49 different polymers from 11 different publications, which were processed by a Python script for data transformation and modelling (See script in ESI).†

3 Transformations

Making a direct connection between conductivity and polymer characteristics can be considered a Sisyphean task. Small alterations in the ionomer, such as changing the ion exchange capacity (IEC), can impact conductivity in many subtle, and sometimes conflicting, ways. Accepting this complexity and drawing connections between the expected relationships creates the diagram depicted in Fig. 3. This figure is divided into three sections: controllable, measurable, and calculable, with arrows illustrating the interaction of one component with another. Controllable refers to parameters that can be changed, such as the environment (temperature and RH) or membrane (IEC, ionomer and morphology). Measurable considers membrane characteristics that can be directly measured as controlled parameters change. Calculable values are those that relate measurable characteristics to membrane conductivity.

Most of the components of Fig. 3 are self-explanatory. However, care should be taken to define the otherwise broad "Ionomer & Morphology" descriptor. Ionomer refers to an individual polymer's molecular form and structure, which defines the presence and arrangement of functional groups, molecular weight, polymer architecture, and other polymeric attributes. Morphology describes the nanoscale structure resulting from the assembly of such molecules into an individual membrane. The ionomer structure is typically controlled by synthesis, whereas morphology is influenced by both the molecular structure and by how a given ionomer is processed into a membrane.

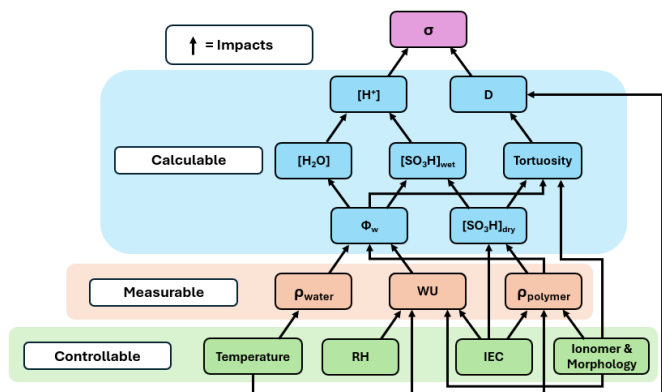


Fig. 3 Framework illustrating the influence of different components on conductivity.

To explain Fig. 3, each component will be discussed in turn. When observed, PFSA-HC differences are noted to gain a better understanding of the conductivity gap's origins and how it can be bridged.

3.1 Density of water, ρ_{water}

The only factor influencing pure water's density is temperature, which causes the density to decrease as it rises. The dataset for this analysis contains results measured at 80 °C. The density of water at 80 °C is 0.972 g/mL.

3.2 Water uptake, WU

Water uptake is the mass of water within a membrane divided by the mass of dry membrane. Temperature, relative humidity, IEC, ionomer, and morphology all have an effect on water uptake.¹³

Temperature has a subtle effect on water uptake, but this is not the focus of this study. Nevertheless, the relationship between temperature and WU can be described using Park's widely utilised water vapour adsorption model.^{41–45} The model incorporates the water clustering equilibrium constant (K_A) and Henry's Law constant (K_H). The clustering equilibrium constant characterises the formation of hydrogen-bonded water clusters. Since bond formation is an exothermic process, increasing the temperature reduces the value of the equilibrium constant, and consequently the WU. Conversely, Henry's Law constant tends to rise with temperature, resulting in higher WU.

RH defines the activity of water in the environment in which the membrane is held. This affects WU because water moves from areas with higher water activity to areas with lower water activity. As a result, increasing RH (*i.e.* increasing water activity of the surrounding vapour) drives water into the membrane (lower water activity), as indicated by a higher WU. This relationship is illustrated in Fig. 4. Also shown Fig. 4, higher IEC correlates with higher WU. IEC represents the sulfonic acid content of the membrane. Given that the acid is hygroscopic, membranes with a higher sulfonic acid content can absorb more moisture. As a result, at any given RH, the membrane with the greatest water absorption capacity will have the highest WU.

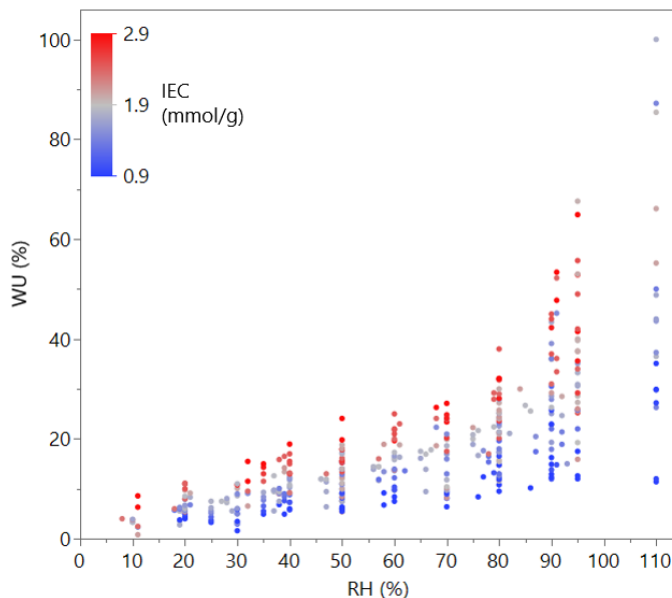


Fig. 4 Water uptake at 80 °C against relative humidity, data at 110% RH represents measurements in water. Marker colour represents the ionomer IEC according to the inset colour scale. Data taken from references 5,7–31.

Ionomers and morphology, like RH and IEC, can affect WU by influencing water solubility within the membrane. Ionomers or morphology that increase the solubility of water in the membrane will have a higher water uptake. This claim is supported by Fig. 4,

where at a given RH, a wide range of WU uptakes can be observed with the same IEC, demonstrating that WU is impacted by membrane properties beyond IEC. Though Fig. 4 provides an opportunity to compare the water solubility of HC and PFSA ionomers directly, it is forgone in favour of water volume fraction in Section 3.4.

3.3 Density of polymer, $\rho_{polymer}$

For polymer density, no studies have reported the density beyond room temperature (20-25 °C). Despite studying data collected at 80 °C, the polymer density used is from room temperature. This is a reasonable approximation as the thermal expansion coefficient of polymers like PTFE and PES would represent less than 1% dimension change when heating the membranes from room temperature to 80 °C. Nonetheless, it is a potential source of error in this analysis.

Ionomer type also makes a significant contribution to polymer density, with published HC ionomer densities ranging from 1.2 to 1.6 g/mL and PFSA densities ranging from 1.9 to 2.1 g/mL.^{10,13,17,21,22,28,46,47} This distinction will be reiterated in the following sections because it is important in all of the calculable components of conductivity. The reason for PFSA materials being denser than HC materials is related to the higher content of heavy atoms (*i.e.* fluorine rather than hydrogen) in PFSA membranes (based on the density difference between polytetrafluoroethylene and polyethylene).

Since ionomer density is seldom quoted in publications, it was necessary to use the estimation method established by Takamuku *et al.*, where density is related to the IEC.³⁸ This analysis expanded the estimation beyond the original dataset to include all ionomers investigated. The original linear relationship observed by Takamuku *et al.* and the expanded relationship are shown in Fig. S4 of the ESI.[†]³⁸

IEC is evident in the density estimation, as higher IEC polymers produce denser membranes. The higher frequency of heavy atoms (*i.e.* sulfur and oxygen, rather than H) and/or tighter ionomer packing as IEC increases are thought to be responsible. Although unproven experimentally to date.

3.4 Water volume fraction, Φ_w

Water volume fraction is the volume of water within a membrane, expressed as a fraction of the membrane's total volume. As a metric, the water volume fraction is more relevant than water uptake to the membranes properties. This is evident within the units of conductivity (mS/cm), where the 'per centimetre' represents distance travelled per cross sectional area ($\frac{cm}{cm^2}$).

The density of the dry membrane (polymer) and water, as well as water uptake, all have an impact on the water volume fraction.^{13,47} The relationship is described mathematically in equation (1):

$$\Phi_w = \frac{V_{H_2O}}{V_{H_2O} + V_{polymer}} = \frac{WU \times \rho_{polymer}}{\rho_{H_2O} + (WU \times \rho_{polymer})} \quad (1)$$

Where $\rho_{polymer}$ and $V_{polymer}$ refer to the density and volume of a dry polymer membrane, respectively. V_{H_2O} is the volume of

water within the membrane when swollen. Assuming constant temperature, water volume fraction will rise as water uptake and polymer density increase. This behaviour is illustrated in Fig. 5.

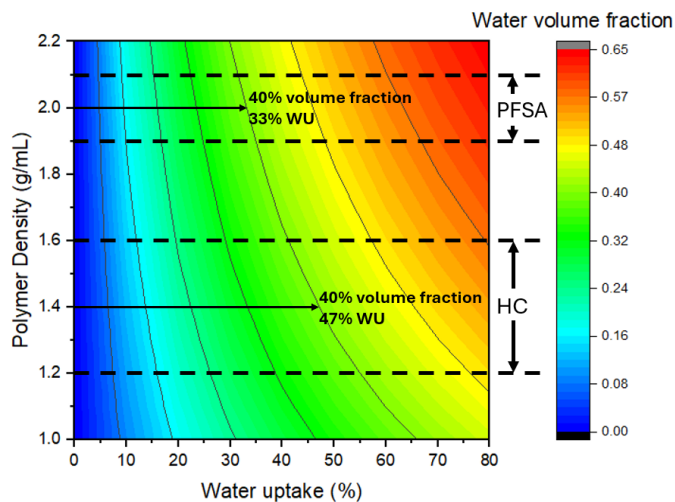


Fig. 5 Water fraction at 80°C as a function of water uptake and polymer density. Dashed lines indicate the observed density range of PFSA and HC ionomers. Arrows draw attention to the water uptake difference when water fraction is constant.

A common observation in published HC studies is that HC ionomers have a higher water uptake than PFSA ionomers.^{5,7-9,25,28,48} This is attributed to two factors, the lower density of HC ionomers and the higher average acid content of HC ionomers. The effect of density on WU is illustrated in Fig. 5 with arrows. The two arrows, representing an HC and a PFSA of equal volume, absorbing the same volume of water. However, because the less dense HC weighs less than a PFSA (at the same volume), water makes up a greater proportion of the HC membrane's mass. As a result, a membrane with a lower density will exhibit a bias towards higher water mass uptake.

Using water volume fraction the density bias is removed. However, the average HC ionomer in this dataset still exhibits a higher water volume fraction across the RH range (data shown in Fig. S5 of ESI).[†]Fig. Inspecting the dataset's IEC reveals that the average HC IEC is 1.89 mmol/g while the average PFSA IEC is 1.08 mmol/g. As discussed in Section 3.2, higher IEC leads to higher water solubility. Therefore, the higher average water volume fraction of the HC ionomers could be the product of higher average water solubility. By trimming the HC ionomer dataset to only include materials up to the highest acid content in the PFSA dataset (*i.e.* make the average acid content the same for both PFSA and HC ionomers) any bias caused by higher average IEC is removed. The trimmed dataset (Fig. 6) of water volume fraction against RH shows no significant difference between ionomer types. This demonstrates that the ionomer type, whether HC or PFSA, has a negligible effect on the water volume fraction when compared to the influence of an ionomers' sulfonic acid contents. Instead, the membrane's acid content has the greatest influence on the water fraction at any given RH.

Relative humidity (RH) is commonly used as the independent

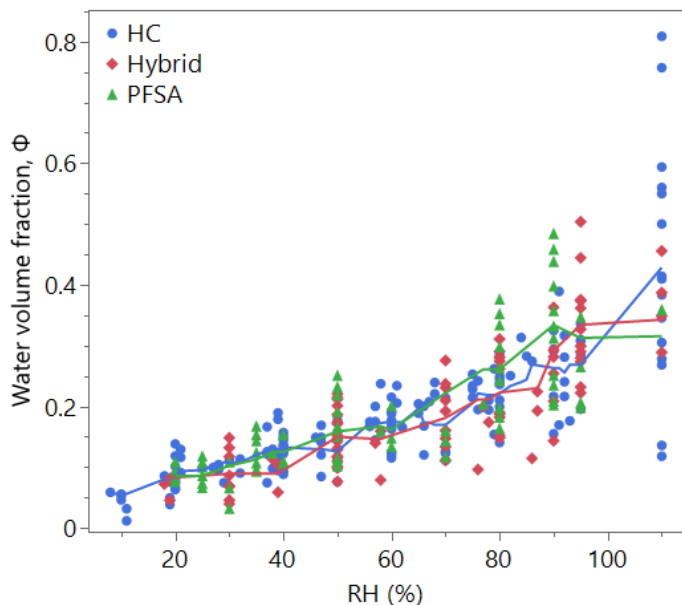


Fig. 6 Water volume fraction at 80 °C against RH. Marker color and shape indicate the type of polymer. Trend lines illustrate moving average. Only membranes with an $[RSO_3H] < 3.6$ are included ($[RSO_3H]$ discussed in Section 4. Data taken from references 5,7–31. Alternative version plotting water volume fraction against lambda is shown in Fig. S6 of the ESI.

†

viable (x-axis) when comparing conductivity of various materials. This is a useful perspective for industries because it informs fuel cell stack designers as to what conductivity to expect if the system is run at a given RH. It is not, however, a suitable perspective for comparing ionomer types. As previously stated, the amount of water absorbed is determined by the RH and the acid content of a membrane. To capture both influences and focus on ionomer differences, the term water fraction will be used for the x-axis in the remainder of this analysis rather than RH.

3.5 Dry membrane sulfonic acid concentration, $[RSO_3H]$

The dry membrane sulfonic acid concentration, or acid content, is the product of IEC and dry polymer density (mmol/mL). Section 3.4 discussed how it affects water fraction, demonstrating its importance in membrane properties. As such, it will be used to separate acid content from other ionomer and morphology influences.

4 Proton concentration, $[H^+]$, and acidity

With a method for determining water volume fraction and acid content established, the next step is to demonstrate how these relate to conductivity. In PEMs, conductivity through a membrane is defined by the concentration of protons and the rate at which these ions move in an electrochemical gradient. This is expressed in the Nernst-Einstein relationship as shown in equation (2):

$$\sigma_{H^+} = \frac{D_{H^+} [H^+] F^2}{RT} \quad (2)$$

Where σ_{H^+} is the proton conductivity, D_{H^+} is the proton dif-

fusion coefficient, $[H^+]$ is the proton concentration in mmol/mL, F is the Faraday constant, R is the ideal gas constant, and T is temperature in kelvin. The use of equation (2) is a potential error source in this analysis as it is a dilute solution expression and does not include nuances associated with the internal membrane environment.^{49–51}

Conductivity is measurable, typically through electrochemical impedance spectroscopy, and was obtained alongside WU from the publications used in this analysis. However, to understand the conductivity gap, it is critical to separate conductivity into its two components: proton concentration and diffusion. Since proton concentration and diffusion are unknown, one must be estimated in order to calculate the other. Proton concentration, the theoretically simpler value due to its direct relation to IEC, was chosen for estimation. The following section discusses the rationale for this approach, as well as whether acidity has an effect on proton concentration.

4.1 Proton concentration limited regime

The proton concentration within a membrane will be limited by one factor under a given regime. This analysis considers three regimes: water limited, dissociation limited, and acid limited. A water-limited membrane is one that contains an excess of acid sites that can dissociate if more water is present. Dissociation limited refers to a system in which there are more water molecules than acid sites, but thermodynamics limits *i.e.* equilibrium constant) the total number of acid sites that dissociate to produce protons. Lastly, acid limited refers to a membrane with all acid sites dissociated, indicating that the proton concentration is limited by the acid concentration. Each regime represents a limiting case, where the proton concentration within a membrane will be defined by the regime of the lowest concentration. The equations that describe each regime are given below:

The water limited regime in equation (3):

$$[H^+] = \frac{\rho_{H_2O}}{M_{H_2O}} \times \Phi_w \quad (3)$$

Where M_{H_2O} is the molar mass of water.

The dissociation limited regime in equation (4):

$$[H^+] = \sqrt{K_a} \times \sqrt{\frac{\rho_{H_2O}}{M_{H_2O}} \times \Phi_w} \times \sqrt{[SO_3H]_{dry} \times (1 - \Phi_w)} \quad (4)$$

Where K_a is the acid dissociation constant.

The acid limited regime in equation (5):

$$[H^+] = [SO_3H]_{dry} \times (1 - \Phi_w) \quad (5)$$

Equation (3) uses the density of water. For this analysis the density of bulk water at 80 °C is assumed. However, a publication by Bai *et al.* shows this a poor assumption as water in the membrane only exhibits bulk water density when lambda is greater than 6.⁴⁷ As the density of water within the different polymers of this analysis is unknown this effect cannot be accounted for. The impact of this uncertainty is minor for the proton concentration as the increased density is offset by the lower water volume fraction, as shown in Fig. S7 of the ESI.†

Of the three, the only equation affected by acidity is the dissociation limited regime. This provides an opportunity to investigate previous publications' claims that, despite the significant acidity difference between the HC and PFSA ionomers, no change in proton dissociation is observed.^{2,12,48,52} To explore this an estimation of the dissociation constant is made using small molecule acids similar to the sulfonic acid groups present within the membrane. As shown in Table 1, all three acids demonstrate high acidity and are considered⁵³ to be strong acids with a K_a greater than 1. Despite all being strong acids, the difference between triflic acid and benzenesulfonic acid (representing PFSA and aromatic HC ionomers, respectively) is exceedingly large. Using the K_a values from Table 1, all three regimes can be plotted onto Fig. 7.

Table 1 pK_a and K_a values for different small molecule analogues. Values taken from Guthrie⁵⁴ and Trummel *et al.*⁵⁵

Molecule	pK_a	K_a
Methanesulfonic acid	-1.9	79.2
Benzenesulfonic acid	-2.8	630
Triflic acid	-14.7	4.84×10^{14}

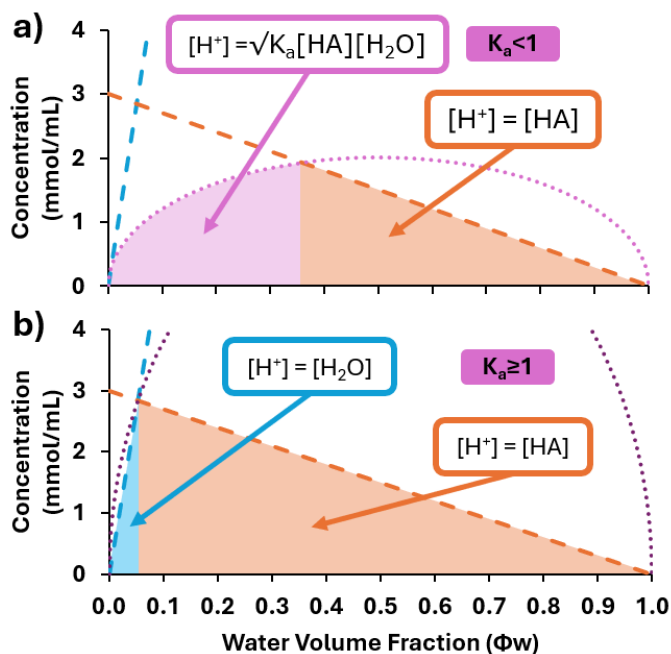


Fig. 7 Acid concentration, $[H^+]$, as a function of water fraction, Φ_w , of an example membrane with a dry sulfonic acid concentration of 3 mmol/mL. a) Represents a membrane with an acid dissociation constant less than 1. At low water fractions the total proton concentration is limited by the proton concentration shaded in pink. At higher water fractions the proton concentration is acid limited, shaded in orange. b) Represents a membrane with an acid dissociation constant greater than or equal to 1. At low water fractions the total proton concentration is limited by the water concentration, illustrated by the blue region. At higher water fractions the proton concentration is acid limited, shaded in orange.

Fig. 7 shows that the concentration of protons within a membrane depends on two factors: the water fraction and the dissociation constant. When the acidity is less than 1 (Fig. 7a), the proton

concentration is determined by dissociation when the water fraction is low and the acid-limited regime when the water fraction is high. In this case, an ionomers acidity is critical for maximising the number of protons available for conduction, since increasing K_a increases the number of dissociated acids. As K_a reaches and exceeds 1, the dissociation limited regime no longer defines the proton concentration. This is because acids dissociate as soon as there are enough water molecules to do so. As such, the proton concentration in Fig. 7b is limited either by the concentration of acid, or the concentration of water.

Table 1 shows that all observed K_a values exceed one. As a result, the proton concentration for all sulfonic acid membranes can be described using the water and acid limited regimes, in which acidity has no effect. This supports the previously stated claim that proton dissociation in HC and PFSA ionomers is similar despite the significant acidity difference. It also is used as the justification for not including acidity as a direct component in the relationship framework of Fig. 3. Instead the components of proton concentration are the water and acid concentration at a given water fraction. Since the water concentration is effectively fixed (other than changing the density of water), the only way to increase proton concentration is to increase acid concentration. This can be achieved by increasing either the membrane density or the IEC. Though acidity does not impact proton concentration, it may influence proton diffusivity. This is discussed in section 6.2.

Having defined proton concentration as a function of water volume fraction, this analysis calculates the diffusion coefficient to better understand the HC-PFSA conductivity gap.

5 Proton diffusion coefficient, D_{H^+}

The proton diffusion coefficient (cm^2/s) refers to the movement of protons through a cross sectional area per second. Higher diffusion coefficients result in more protons crossing per second. This should not be confused with proton concentration, as it is unrelated to the total proton content and only relates to the rate at which protons cross the membrane. This provides insight into conductivity after the impact of proton concentration has been removed. In other words, membranes with the same structure but different acid concentrations should have the same diffusion coefficient, even if the measured conductivity varies.

The diffusion coefficient can be calculated by using equation (2), with proton concentration calculated from equation (5) (unless the water fraction is low), and the conductivity taken from published data. The calculated diffusion coefficients are plotted in Fig. 8 against water volume fraction, revealing a subtly different relationship when compared to the conductivity-RH relationship seen in Fig. 1. The greatest difference between PFSA and HC ionomers for both figures is seen when the water fraction is low. Since the diffusion coefficient removes proton concentration effects it can be stated that the conductivity gap is caused by slower proton diffusion in HC membranes during dry conditions. Though this directly answers the conductivity gap question, it provides no clarity as to why HC membranes exhibit lower diffusion coefficients. To probe into this disparity, the parameters affecting diffusion are broken down into three factors: temperature,

tortuosity, and diffusion mechanism.

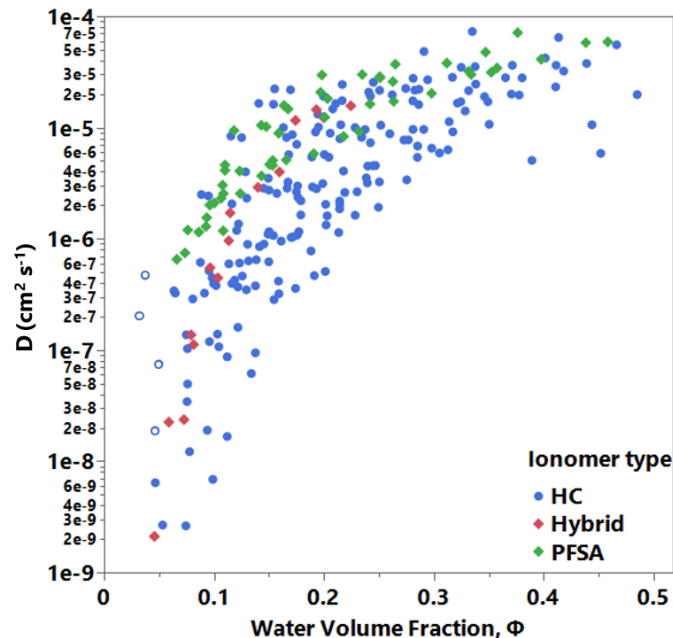


Fig. 8 Diffusion coefficient, D , against water volume fraction, Φ_w at 80 °C. Marker colour and shape represent the polymer type. Data taken from references 5,7–31. Hollow markers represent diffusion coefficients calculated for a membrane in a water limited regime.

Ionomers labelled 'Hybrid' are neither PFSA nor HC, as the ionomer contains fluorine but not the groups characteristic of a PFSA.

Diffusion is thermally activated, the diffusion coefficient of ions will increase as the temperature increases, as explained by Nuernberg.⁵⁶ Though the influence of temperature is significant, the dataset considered within this analysis represents data collected at 80 °C exclusively. As such, the contribution of temperature is not explored any further as the source of the conductivity gap.

The second factor is tortuosity, defined as the distance a proton must travel to cross the membrane divided by the membrane thickness. A membrane where the proton can travel straight from one side to the other will have a tortuosity of 1. As kinks and bends are added to the protons path, the tortuosity value increases. The relationship between the diffusion coefficient and tortuosity can be estimated using equation (6):^{57–60}

$$D_{H^+} = \frac{D_{H^+}^\ominus}{\tau} \phi_w \quad (6)$$

Where τ is tortuosity, ϕ_w is water volume fraction available for diffusion, and $D_{H^+}^\ominus$ is the diffusion coefficient of a proton in an infinitely dilute acid (constant). This analysis, which divides the membrane into two parts, water and polymer, assumes that proton diffusion occurs primarily in the water part rather than in the polymer. Therefore, ϕ_w is used in equation (6) instead of porosity as the membranes are not porous media. When the diffusion coefficient is plotted against the water fraction, the result is a linear equation with a zero intercept and a gradient proportional to the tortuosity. Attempting to use this equation to model the results in Fig. 8 produces poor fits, as the relationship between

the diffusion coefficient and the water fraction is not linear. This means that a factor beyond tortuosity is influencing the diffusion coefficient.

The final factor is diffusion mechanism, which describes the process by which a proton can move through a membrane. Numerous publications have shown that protons can travel through the membranes in many different ways. Examples include vehicular and Grotthuss, with the dominant mechanism depending on the membrane and its degree of hydration.^{6,7,12,13,52,61–70} Generally, protons move more slowly when interacting with a sulfonate (deprotonated sulfonic acid) and more rapidly when not. Since the sulfonate groups are immobile, any ionic interactions between protons and sulfonate groups will hinder the protons' movement across the membrane. Weakening these ionic interactions makes proton movement less restricted and increases the diffusion coefficient. Additionally, water plays a pivotal role in minimizing the ionic interactions by shielding the ionic charges (*i.e.* each water surrounding a sulfonate or proton screens the charge, meaning the ions must come closer together to interact).^{52,71–79} This divides the various mechanisms into two broad categories: slower diffusion when interactions are predominate, and faster diffusion when the interaction is minimized by water. The duality of fast versus slow diffusion is evident from Fig. 8. Starting with low water fractions and gradually increasing: an initial slow diffusion coefficient, a transition to fast diffusion as charges are shielded, and a final steady diffusion coefficient after the sulfonate-proton interaction cannot be reduced any more with additional waters.

To model the transition from slow to fast mechanisms, the following assumption is made: fast mechanisms dominate when the membrane contains a bulk-water network. Bulk-water refers to any water within the membrane that is not polarized by the electrostatic field surrounding each charged sulfonate. A bulk-water network refers to a network of bulk-water domains that intersect across an entire membrane. The formation of the bulk-water network is key, as any isolated bulk-water regions would be throttled by the slower diffusion in the polarised water regions surrounding them (*i.e.* protons move quickly through the bulk-water, but the average diffusion will be limited by the slower diffusion occurring in the polarised water before/after the bulk-water pocket).

The assumption that bulk-water networks are required for fast diffusion mechanisms to dominate is supported by freezing differential scanning calorimetry, which observes freezable (bulk) water only at water fractions immediately following the slow-to-fast diffusion coefficient transition.^{7,13,80} An example of this relationship calculated from data published by Mochizuki *et.al.* is provided in the Fig. S8 of ESI.^{†7} Accepting that bulk-water network formation coincides with the onset of fast diffusion, the next step is to describe the bulk-water network formation by applying percolation theory to the data in Fig. 8.

5.1 Percolation theory

Percolation theory is used to describe property changes as a network evolves within a material. The Sahimi⁸¹ illustration of percolation theory describes how the percolation of roads connecting different locations in a town determines whether cross-town

travel is possible as the number of open roads changes. For example, with all roads open, the network is continuous, allowing an individual to freely traverse around town. As roads are closed, the network becomes less interconnected, making cross-town travel more frustrating but still possible. As the number of closed roads reaches a critical threshold value, cross-town travel becomes impossible since the once continuous network becomes non-continuous. In this example, the critical threshold is determined by the degree of road percolation. Highly percolated networks remain continuous even after many roads are closed, whereas poorly percolated networks become non-continuous after only a few roads close. Applying this example to the bulk-water network formation, the water fraction represents the "open-roads" in the membrane, and the diffusion coefficient describes the ease of travel across the membrane.

In terms of conductivity, classical percolation theory describes a system that goes from insulator to conductor or conductor to superconductor.^{81,82} The conductor to superconductor transition does not apply to membranes because resistance occurs regardless of whether a bulk-water network exists. The insulator to conductor transition is also problematic because it implies that a membrane that does not contain bulk water is an insulator. This is not true, considering that conductivity is measurable when no bulk-water is observed.^{7,13,80} Therefore, an alternative conductor-conductor model must be used.

Generalized Effective Medium (GEM) theory is a hybrid model which combines percolation theory with Effective Medium Theory (EMT).^{39,83-86} EMT is used to simulate the macroscopic properties of composites by averaging all of the inhomogeneous components with different microscopic properties into a single macroscopic property.^{40,81,82,84} When applied to a membrane, EMT describes the averaged proton diffusivity across both non-bulk-water and bulk-water components. At low water fractions, non-bulk water dominates the averaged diffusivity. As the water fraction increases, the faster proton diffusion through the bulk-water network component significantly increases the averaged diffusion coefficient. The percolation theory component describes the bulk-water network formation. Mathematically, the GEM theory can be described^{39,84,87} by equation (7):

$$\Phi_w \times \frac{(D_w^{1/t} - D_{\Phi_w}^{1/t})}{D_w^{1/t} + AD_{\Phi_w}^{1/t}} + (1 - \Phi_w) \times \frac{(D_p^{1/t} - D_{\Phi_w}^{1/t})}{D_p^{1/t} + AD_{\Phi_w}^{1/t}} = 0 \quad (7)$$

Where D_w is the proton diffusion coefficient as the membrane tends to infinite dilution, D_p is the diffusion coefficient as the membrane tends to complete desiccation, D_{Φ_w} is the diffusion coefficient at a given water fraction, t is the percolation exponent, and A is $\frac{\Phi_c}{1-\Phi_c}$ and is rearranged to produce the critical percolation threshold (Φ_c) for this analysis. Fig. 9 illustrates the general shape of a curve produced by the GEM model, and how each parameter affects the curve shape. In terms of the two models, EMT describes the diffusion coefficient at the minimum and maximum water fraction (D_p and D_w). Percolation theory describes the transition in-between, with the critical percolation threshold representing the water fraction when the diffusion coefficient change is greatest, and the percolation exponent is illustrating the gen-

eral shape of the curve.

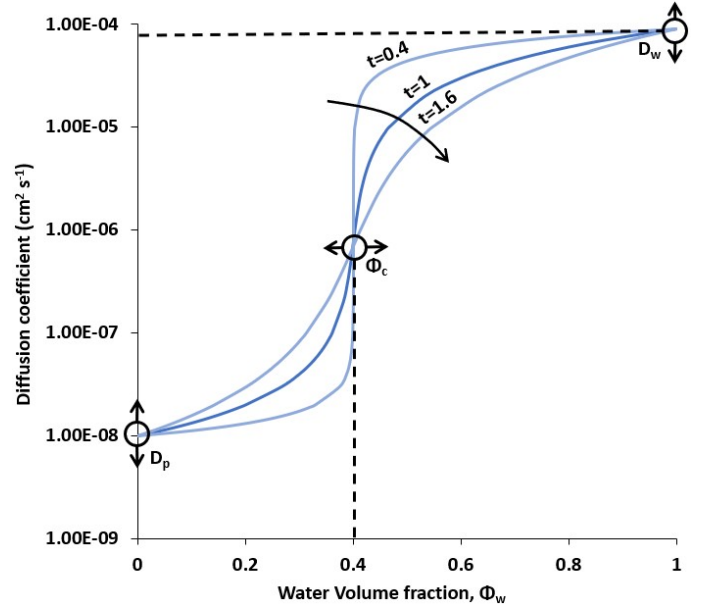


Fig. 9 Example GEM curve (in blue) with $\Phi_c = 0.4$, $D_p = 1 \times 10^{-8}$, $D_w = 9 \times 10^{-5}$, and $t = 1$. The other (greyed) lines represent the same parameters except $t = 0.4$ and $t = 1.6$ for the upper and lower lines, respectively. Arrows indicate the change caused by altering the respective parameter (D_p and D_w change the diffusion coefficient when water volume fraction is 0 and 1, respectively. Φ_c changes the water volume fraction at the midpoint).

To model the dataset with GEM, this analysis used the Python fitting package "lmfit".⁸⁸ To fit each dataset lmfit uses the Levenberg-Marquardt method.^{89,90} The Python script, initialization, and boundary parameters for these fits are provided within the Table S1 of ESI.†

Returning to the HC-PFSA proton diffusion difference, the next step is to look into how the GEM fitting parameters explain the differences between the ionomers.

6 Discussion

6.1 Critical percolation threshold (Φ_c)

Critical percolation threshold represents the water fraction at which a continuous bulk-water network exists across the membrane. A higher percolation threshold indicates that a membrane requires a greater volume of water to establish a bulk-water network compared to a membrane with a lower percolation threshold. Examining the percolation thresholds produces a correlation with an ionomer's acid concentration, as shown in Fig. 10. Membranes with higher acid concentrations exhibit a critical percolation threshold at a greater water fraction.

To describe the relationship a parameter lambda (λ) is used to quantify the number of water molecules per sulfonate group, shown in equation (8).

$$\lambda_{\Phi_c} = \frac{[\text{H}_2\text{O}]_{\Phi_c}}{[\text{RSO}_3\text{H}]} \quad (8)$$

λ_{Φ_c} is the number of water molecules per sulfonate group at the critical percolation threshold, $[\text{H}_2\text{O}]_{\Phi_c}$ is the water concentration

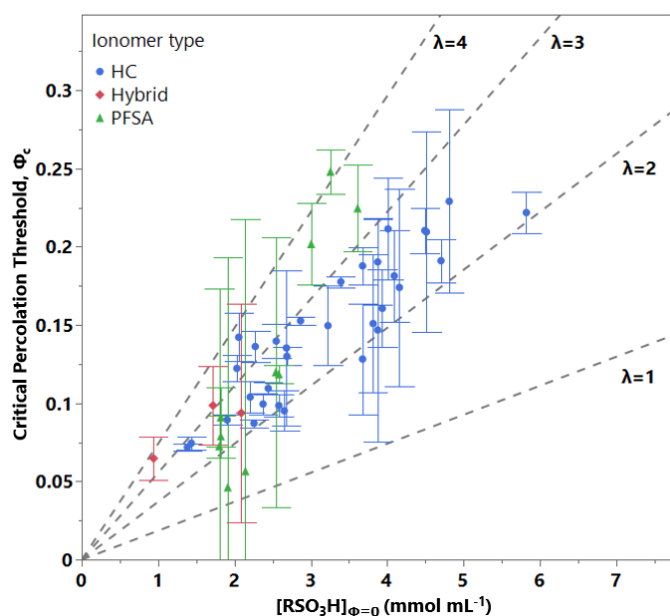


Fig. 10 The critical percolation threshold against sulfonic acid concentration in the dry membrane. Data colour and marker represents the ionomer type. Data from references 7,9,11,12,20,21,23–25,28,31,33 Lines illustrate the expected relationship for different lambda (λ) values, which are defined as the number of water molecules per sulfonate group. Error bars represent fitting intervals of one standard deviation from the best fit.

at the critical percolation threshold, and $[\text{RSO}_3\text{H}]$ is the dry membrane acid concentration. This can be related to Φ_c by combining equation (8) with equation (9), producing equation (10).

$$\Phi_c = \frac{[\text{H}_2\text{O}]_{\Phi_c}}{[\text{H}_2\text{O}]_{\text{water}}} \quad (9)$$

$$\Phi_c = \frac{\lambda_{\Phi_c}}{[\text{H}_2\text{O}]_{\text{water}}} \times [\text{RSO}_3\text{H}] \quad (10)$$

$[\text{H}_2\text{O}]_{\text{water}}$ is the molarity of water at 80 °C. Since water molarity is constant, the expected relationship for the critical percolation threshold is a linear increase with acid concentration. Steeper linear gradients are the product of higher λ values. Example responses for λ values between 1 and 4 are plotted in Fig. 10. From this perspective the majority of the points in the dataset, irrespective of ionomer type, show percolation thresholds between $2 < \lambda < 4$. The universality is illustrated when diffusion coefficient is plotted against λ in Fig. 11 where the diffusion coefficients of HC and PFSA ionomers converge between λ values of 2 and 4. This mirrors publications where the observed λ value for acid charge shielding is also between 2 and 4.^{52,71–73,91–94} The correlation between these observations adds support to the GEM parameters' capacity to describe bulk-water network formation and the resulting change in diffusion coefficient.

The agreement of the GEM calculated critical percolation threshold and observed λ values suggests that GEM can accurately describe the water network better than previous studies using the classical percolation model.^{58,59} In these studies, the percolation threshold tended to 0, which is significantly smaller than the GEM results and the mathematical literature.⁹⁵ In partic-

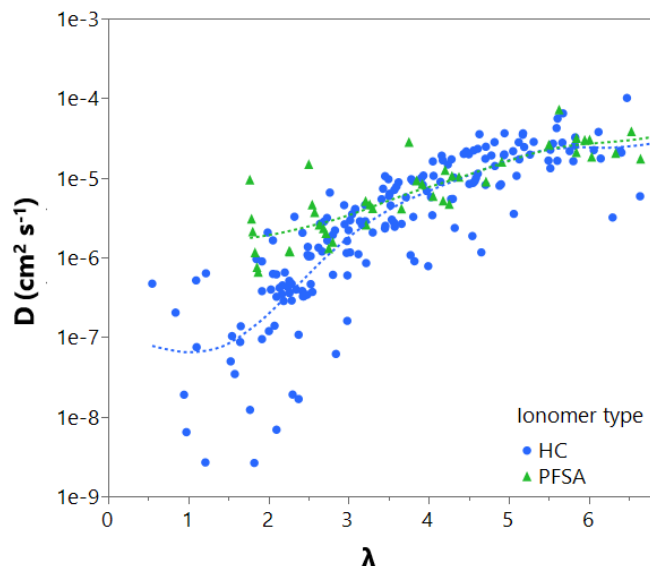


Fig. 11 Diffusion coefficient of HC and PFSA membranes against λ . Data colour and marker represents the ionomer type. Data from references 7,9,11,12,20,21,23–25,28,31,33 Spline curves are added to illustrate trends. The hybrid materials are excluded due to small dataset (3 polymers), version including Hybrid materials is available in Fig. S8 of the ESI.†

ular, Ochi *et al.* suggests that the discrepancy observed between the classically modelled results and theoretical results is because the classical model assumes "only the water region contributes to the conduction pathways".⁵⁸ GEM avoids this assumption by modelling the protons as slower when interacting with sulfonate groups, or faster when diffusing through bulk-water.

Fig. 10 shows that all ionomers, regardless of type, need a similar number of water molecules per sulfonate to form a bulk-water network. Fig. 10 also shows that low acid-content membranes exhibit a lower critical percolation threshold. This implies that these membranes require less water to form a bulk-water network, suggesting a potential lower RH transition to fast proton diffusivity. However, this does not account for a membrane's affinity to water (hygroscopicity), as discussed in section 3.4. As illustrated in Fig. 12, membranes with low critical thresholds do not have higher low-RH diffusivity, instead exhibiting slower proton diffusion. This can be explained by the fact that membranes with a high acid content have a higher water affinity, resulting in a larger water fraction at any given RH. This offsets the higher critical water fraction threshold, leading all membranes, regardless of acid content, to form a bulk-water network at a similar RH (15-35% RH). The relationship between proton diffusion and acid concentration accounts for the lower critical thresholds' lower proton diffusivity. This is discussed in Section 6.2.

From the critical percolation threshold, the following is ascertained. First, that all ionomers are forming the bulk-water network at similar λ values. Second, a high critical percolation threshold requires more water in the membrane to form the bulk-water network. Third, despite the acid content increasing the water fraction required for a diffusive network, the increasing hygroscopicity associated with a higher acid content overshadows

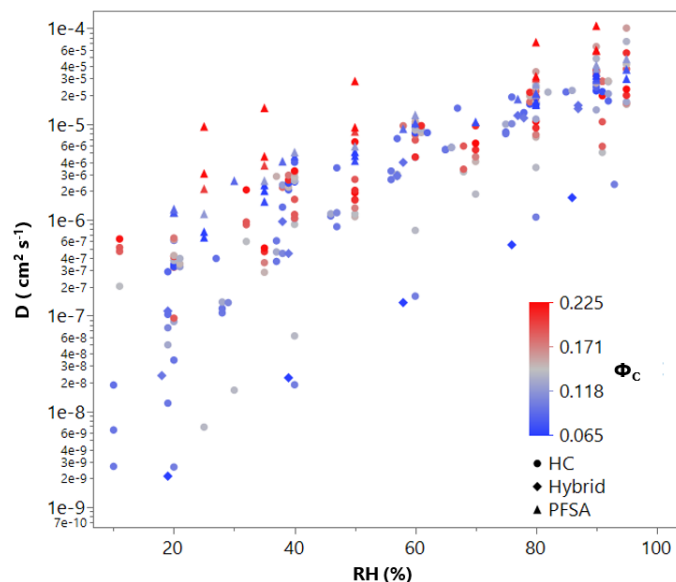


Fig. 12 Diffusivity against RH. Data colour represents the critical percolation threshold calculated from GEM, values indicated by colour bar. Marker represents the ionomer type. Data from references 7,9,11,12,20,21,23–25,28,31,33

the higher water fraction requirement. Although none of these findings help to understand the HC-PFSA conductivity gap, they do illustrate how the change in the IEC or density of an ionomer affects the formation of a water network within the membrane.

6.2 Diffusion coefficient without a bulk-water network (D_p)

Having discussed the water fraction at which a bulk-water network forms, and concluding that it does not explain the conductivity gap, the next step is to explore the diffusion coefficient before the bulk-water network. This can be described by the GEM parameter D_p , which is the diffusion coefficient of protons through a membrane as the water fraction tends to 0. To clarify, this analysis does not suggest that proton conduction can occur in a completely desiccated membrane. Instead D_p is used to describe proton diffusivity when the membrane is in a water limited regime, as described in section 4.1. Under this regime, any proton will exist as a hydronium and sulfonate ion pair. Therefore, diffusion occurs by the slower diffusion mechanisms associated with strong ionic interactions. To empirically support the possibility of proton conduction in the water-limited regime, publications are cited here as examples of conduction when $\lambda < 1$.^{8,12,14,20,23,46}

Fig. 8 supported the idea that inferior dry-HC conductivity is caused by slower proton diffusivity when compared to PFSA ionomers. Using D_p , this idea can be illustrated as the correlation between low RH conductivity and D_p as shown in Fig. 13. In this case, all polymers follow the same trend: increasing proton diffusivity increases conductivity by an equal amount. The materials with the highest conductivity (PFSA ionomers) have the highest D_p . Therefore, increasing the D_p of HC ionomers should improve their dry conductivity. As HC ionomers display a wide array of D_p values, the data enables an exploration into different dry conductivity improvement strategies.

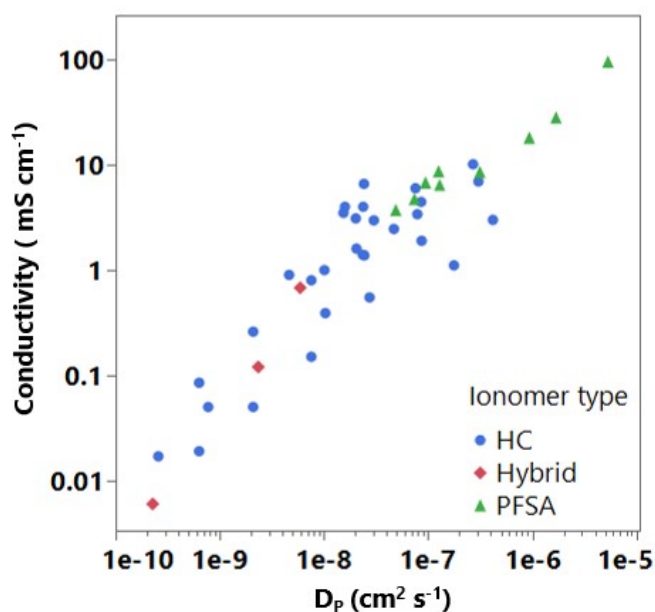


Fig. 13 The conductivity of membranes between 8% and 26% RH against the D_p of the respective polymer. Marker colour and marker represents the ionomer type. Data from references 7,9,11,12,20,21,23–25,28,31,33

This analysis discusses how polymer design influences D_p using case studies based on data sets from selected publications. For transparency, all D_p values are plotted in Fig. 14, with the notable case studies highlighted and connected.^{11,20,21,24,31} As a general trend, the highest D_p values are associated with PFSA, then HC, though there is significant overlap across both ionomer types.

The first case study is based on a study by Maalouf *et al.*²⁴ In this publication, the IEC of 3M PFSA ionomer is varied. This is achieved by changing the average number of tetrafluoroethylene (TFE) spacer groups between each sulfonic acid side chain. Labeling the TFE groups as hydrophobic, and the sulfonic acid side chains as hydrophilic, Maalouf *et al.* provides a dataset representing polymers with the proportion of hydrophilic groups ranging from 13% to 40%. The observed result of increasing the proportion of hydrophilic groups is an increase in D_p . This is an example for higher acid concentrations making less tortuous proton diffusion pathways. Since D_p represents proton diffusion when charges are not shielded, any proton being transported must be associated with a sulfonate group. Therefore, a less tortuous sulfonic acid network implies a less tortuous diffusion network. This is suggested by Maalouf *et al.* who proposes "tight packing of sulfonates with an appropriate lateral geometry to allow water bridging".²⁴ This observation is also mirrored in publications where classical percolation theory has been applied to the measured conductivity of systems with variable acid content.^{96–101} Only membranes above a critical sulfonic acid content exhibit conductivity. Below the critical acid concentration, there is insufficient sulfonic acid to form a continuous network that protons can diffuse across.

From the Maalouf *et al.* case, the expected response for increasing acid content is less tortuous proton diffusion pathways and higher D_p , irrespective of ionomer. This holds true for the publi-

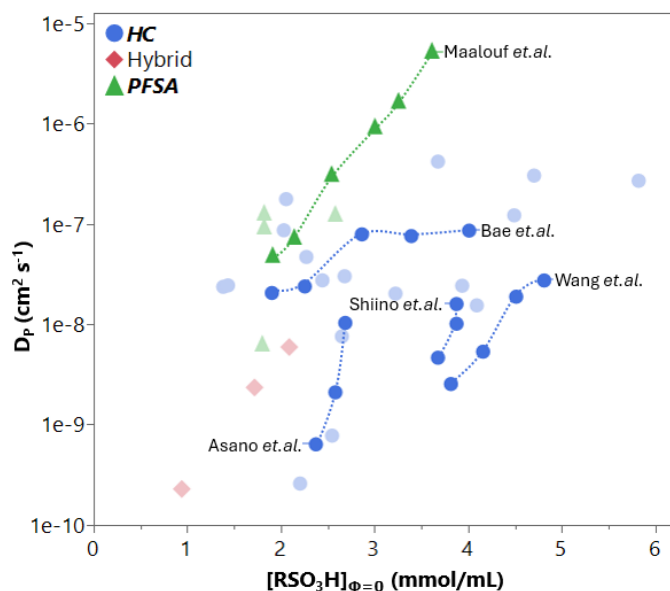


Fig. 14 D_p against dry sulfonic acid concentration. Marker color and shape represent polymer type. Highlighted and connected data to draw attention to different examples discussed. Data from references 7,9,11, 12,20,21,23–25,28,31,33

cation by Wang *et al.* where poly(ether sulfone)s (PES) are synthesized with aliphatic side chains ending in sulfonic acids.³¹ The acid concentration of these membranes is controlled by the percentage of hydrophilic (sulfonic acid containing) to hydrophobic blocks. The published ratios range from 40% to 55% hydrophilic blocks. As with the previous case, increasing the hydrophilic content (increasing acid concentration) decreases tortuosity, leading to higher D_p .

Both PFSA and PES ionomers share the increasing D_p relationship with acid content. However, the D_p of both ionomers, when the hydrophilic group ratio is 40%, reveals more than a 2000 fold difference. Since both ionomers have a similar number of acid groups per unit volume (3.6 and 3.8 mmol/mL for PFSA and PES, respectively), this implies that proton diffusion through the PFSA ionomer is less tortuous. To explain this two factors are considered: the jump distance of a proton and the morphology of an ionomer. Fig. 15 illustrates the influence of each factor. Between Fig. 15A and Fig. 15B, keeping morphology (arrangement of polymer chains) constant and increasing the jump distance decreases tortuosity (shorter black arrow). This can be rationalized with the K_a values provided in Table 1, where the aliphatic sulfonic acid groups of PES are significantly less acidic than the fluorinated PFSA. Though both dissociate completely in the presence of water, the lower K_a means a lesser anionic counter charge screening and a more localised proton.^{6,102} Between Fig. 15A and Fig. 15C the arrangement of chains is changed to reduce the path length and, thus, tortuosity. Examples of morphology change altering diffusivity are numerous, as summarized in the review by Wu *et al.*²

Between acidity and morphology, morphology is the more significant contributor to D_p . Considering the K_a values (Table 1), a system heavily influenced by K_a should exhibit significant D_p

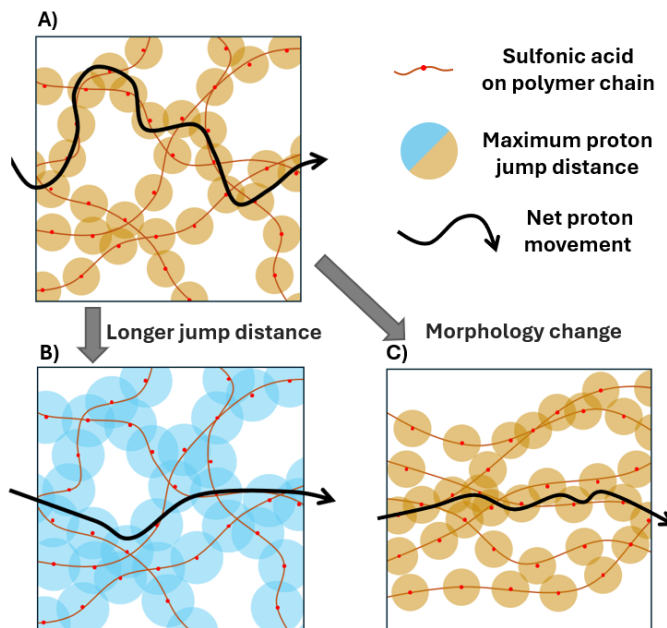


Fig. 15 Illustrations of tortuosity of sulfonic acid sites within polymer membranes. As the the net proton movement arrow becomes less straight it becomes longer, leading to higher tortuosity. A baseline system is shown in A), a system where the proton jump distance is increased is shown in B), a system where the morphology has changed is shown in C).

difference between fluorinated acids and non-fluorinated acids. That is, the considerable more acidity fluorinated acids should exhibit D_p values that do not overlap with the aliphatic and aromatic sulfonic acids. By plotting the D_p of different sulfonate types (see Fig. S10 in ESI)† the data shows some aliphatic and aromatic sulfonic acids exhibiting a higher D_p than the fluorinated acids. This suggests that ionomer acidity is not as effective at improving dry diffusivity as improving the morphology that an ionomer adopts. Therefore, the proton-acid group interactions is not the dominant factor in determining proton diffusivity.

Assuming morphology is the dominant contributor to the D_p difference Kreuer *et al.* shows that the both HC and PFSA ionomers exhibit a "structural motif [that] is quite universal".¹⁰³ Yet "lower tortuosity (on a larger scale), resulting from the larger backbone persistence length characteristic to PFSAs compared to hydrocarbons, may lead to a more efficient percolation within the proton conducting aqueous domain." Summarising, Kreuer *et al.* suggest that both ionomer types phase separate, but PFSA ionomers exhibit less random (regularly structured over longer ranges) hydrophilic channels. Considering both the PFSA and the PES being examined have sulfonic acid group side chains of the same length its likely that this difference originates from the packing of backbones. A publication by Crothers *et al.* suggests that microscale channel-size distribution is has a significant impact on transport properties.⁷⁴ If PFSA channel size distribution is more uniform than HC ionomers then the likelihood of induced local transport gradients will increase, which Crothers *et al.* show decreases conductivity.^{50,51,74} Supporting this are water drag coefficients observations by Pisani *et al.* showing that

the water drag in Nafion remains non-zero when water volume fraction is 0.1.¹⁰⁴ The water drag in the example HC is not measurable below a water fraction of 0.2. Therefore, the influence of local transport gradients from a broader channel size network distribution in the HC ionomer could be used to explain this dramatic difference. If this is true, then increasing the long-range ordering of the hydrophilic domains in HC ionomers may be key to closing the conductivity gap.

Returning to the PES *versus* PFSA ionomers, both show that increasing acid concentration increases D_p . In terms of closing the conductivity gap, this illustrates the first strategy: increasing sulfonic acid concentration. The advantage to this approach is simplicity, as increasing the degree of sulfonation is typically a straightforward synthetic step. The disadvantage of additional acid is the higher water volume fractions that results (as indicated in Section 3.4), especially at a higher humidity. Higher water fractions increase gas crossover, and seriously diminish key mechanical properties like Young's modulus.^{21,28,31,105–107} Therefore, increasing acid content should be done carefully, considering the higher water volume fractions it will cause.

For block-ionomers, an alternative to changing the acid content is changing the size of hydrophilic/hydrophobic blocks. In other words, maintaining the block ratio (*i.e.* 1 hydrophilic for every 2 hydrophobic) but making each block twice the size. This approach maintains a constant acid content whilst manipulating the morphology adopted by a given ionomer. This is exemplified in the report by Asano *et al.*, where a sulfonated polyimide (SPI) is made with different hydrophilic block lengths.²⁰ These data are highlighted in Fig. 14, showing increasing block size from 10 to 40 to 80 as D_p increases with only a small change in acid content. With chemical structure and concentration of acids fixed, the logical explanation for increasing D_p is longer hydrophilic blocks making morphology more conducive to faster proton diffusion. Asano *et al.* obtained stained transmission electron microscopy (TEM) images showing that larger hydrophilic blocks produce better connected ionic domains. This result is corroborated by data from other publications, all finding that longer hydrophilic blocks make for more interconnected acid networks.^{28,36,107} However, this approach is only possible with block polymerization, where the size and ratio of constituents can be controlled.

Shiino *et al.* proposes a different approach to controlling morphology via backbone rigidity.¹¹ Based on a persistence length design principle (proposed by Miyake *et al.*) the rigidity is controlled by the ratio of *para* to *meta* groups in a fully aromatic backbone.¹⁰⁸ The concept is that a polymer comprised entirely of *para* backbone links will be rigid and unable to bend. Adding *meta* linkages to the backbone improves flexibility as it introduces bends into the otherwise rod-like structure. Shiino *et al.* produced 3 polymers with different hydrophilic blocks: SPP-MP (1:1 *meta:para*), SPP-BP (2:2 *meta:para*), and SPP-QP (4:1 *meta:para*). Note, that the study did not control hydrophilic domain size. Since the acid content was fixed, the larger hydrophobic domains (hydrophobic domain size SPP: MP<BP<QP) also produced larger hydrophilic domains (hydrophilic domain size SPP: MP<BP<QP). As a result, this strategy overlaps with the block

size strategy.

Shiino *et al.* studies morphology using stained TEM and small angle neutron scattering (SANS). They conclude that larger hydrophilic blocks decrease the likelihood of isolated ionic domains, a similar conclusion to that based on the work varying ionomer block-size.^{20,23,36,107} As a result, the publication suggests that the greatest influence on conductivity is the inter-connectivity of ionic domains, rather than the rigidity of backbone segments. This observation is supported by a study from Peressin *et al.* who investigated the effects of backbone rigidity on membrane performance.¹⁰⁹ This study finds that backbone rigidity has minimal direct influence on proton conductivity, but does influence it through water uptake. Backbone rigidity increases water sorption, causing proton dilution and weaker membranes. Peressin *et al.* attributes the improved properties to "macroscopic chain entanglement" when backbone flexibility is enhanced. As a result, improving backbone flexibility should be considered as a water uptake reduction strategy, enabling the synthesis of higher IEC ionomers.

As found by the two strategies, increasing acid concentration increases the number of acid sites, improving D_p by reducing tortuosity. Additionally, increasing hydrophilic domain sizes also improves D_p , presumably by increasingly the likelihood that a highly percolated ionic network forms. Bae *et al.* (as highlighted in Fig. 14) illustrates a case where both occur simultaneously. Using a sulfonated poly(arylene ether sulfone ketone) (SPESK) block ionomer, Bae *et al.* increase acid concentration by increasing the size of the sulfonated block whilst the size of the hydrophobic block is kept constant. The result is a large range of acid concentrations, all with similar D_p values. This is contradictory to the previous strategies, whereby more acid and larger blocks should produce higher dry diffusion coefficients. This discrepancy suggests that both outlined strategies may only work for some polymers, and cannot be universally applied. The results of Bae *et al.* could be attributed to rigid and highly sulfonated fluorenylidene biphenylene units (in-fact, multiple publications using this group all exhibit similar D_p values, as shown in Fig. S11 of the ESI).^{7,21,33} This group may limit the morphological development as a membrane dries, resulting in similar morphologies irrespective of acid content or block size. This highlights a limitation of this analysis, namely processing. As shown extensively with PFSA ionomers, processing (*e.g.* casting solvent, annealing, conditioning) the same ionomer differently can lead to significantly different properties.^{13,96,110–116} Less is known about ideal HC processing conditions, but it is likely that the optimal processing will change between ionomers.^{117,118} All HC ionomers discussed in the present analysis should be considered un-optimised, especially in comparison to less diverse PFSA ionomers. Currently, PFSA ionomers adopt a morphology which enables higher proton diffusivity under dry conditions.^{6,7,11,12,62,71,107,119–121} However, it is clear from this analysis that iterative polymer design and process optimization can close the HC-PFSA gap, opening up HC ionomers for use in drier conditions.

6.3 Percolation exponent, t

In fitting the GEM model to the present dataset, the percolation exponent t was acquired. This value describes the transition shape (as shown in Fig. 9) of proton diffusivity from low to high water fractions.^{85,86} For mathematical lattice structures the exponent is universal.^{39,84} For a continuum system where the percolating structure does not fit onto a lattice grid, the percolation exponent is not universal. Currently, it is believed that t is related to the shape of a conducting channel, with shapes such as rods, producing t values as high as 5.8.^{39,85,86} No obvious trends in t were observed in this dataset. Ideally, a relationship could be drawn between the GEM model percolation exponent and the water domain shape or size, as outlined by Crothers *et al.*⁷⁴. This could be achieved by collecting a larger dataset and supporting it with morphological analysis such as small angle scattering or microscopy.

7 Conclusion

This analysis brings together a variety of ionomers from both PFSA and HC materials. Examining all conductivities, it was discovered that HC ionomers can outperform PFSA ionomers in wet conditions but fall short in dry environments; an observation known as the conductivity gap. To understand the source of the gap, the inherent differences between the two material groups were normalised, establishing a clear framework for effective material comparisons. Using the framework, the cause of the conductivity gap was identified as low dry diffusivity of protons in HC ionomers. To describe diffusivity differences, the Generalised Effective Medium Theory (GEM) is used. Using GEM's fitting parameters, it is clear that all ionomers form a percolated bulk-water network at similar water levels, regardless of ionomer type. When compared to the influence of tortuosity and morphology, acidity has a negligible effect on conductivity. In the dry membrane, the morphology of PFSA ionomers is shown to be more conducive to diffusion than HC ionomers, which creates the conductivity gap. Case studies from the analysed literature were chosen to identify various strategies for improving the morphology of HC ionomers to facilitate conduction. GEM was found to be an accurate descriptor of observed diffusion behaviour, agreeing with many experimental and computationally observed results. In the future, the framework and GEM model will be used to evaluate various polymers and to help develop improved ionomers for use in FC and WE applications.

Conflicts of interest

There are no conflicts to declare.

Acknowledgements

The authors thank Johnson Matthey for a PhD studentship to William Bangay.

Notes and references

- 1 PFAS – the 'Forever Chemicals', <https://chemtrust.org/pfas/>, Accessed: 2024-12-04.
- 2 L. Wu, Z. Zhang, J. Ran, D. Zhou, C. Li and T. Xu, *Phys. Chem. Chem. Phys.*, 2013, **15**, 4870–4887.

- 3 H. Nguyen, C. Klose, L. Metzler, S. Vierrath and M. Breiwwieser, *Adv. Energy Mater.*, 2022, **12**, 2103559.
- 4 P. A. García-Salaberri, *SM&T*, 2023, **38**, e00727.
- 5 E. M. W. Tsang, Z. Zhang, A. C. C. Yang, Z. Shi, T. J. Peckham, R. Narimani, B. J. Frisken and S. Holdcroft, *Macromolecules*, 2009, **42**, 9467–9480.
- 6 K. Kreuer, *J. Membr. Sci.*, 2001, **185**, 29–39.
- 7 T. Mochizuki, K. Kakinuma, M. Uchida, S. Deki, M. Watanabe and K. Miyatake, *ChemSusChem*, 2014, **7**, 729–733.
- 8 K. Matsumoto, T. Higashihara and M. Ueda, *Macromolecules*, 2009, **42**, 1161–1166.
- 9 K. Miyatake, T. Shimura, T. Mikami and M. Watanabe, *Chem. Commun.*, 2009, 6403.
- 10 S. Chen, R. Hara, K. Chen, X. Zhang, N. Endo, M. Higa, K. Okamoto and L. Wang, *J. Mater. Chem. A*, 2013, **1**, 8178.
- 11 K. Shiino, T. Otomo, T. Yamada, H. Arima, K. Hiroi, S. Takata, J. Miyake and K. Miyatake, *ACS Appl. Polym. Mater.*, 2020, **2**, 5558–5565.
- 12 E. G. Sorte, B. A. Paren, C. G. Rodriguez, C. Fujimoto, C. Poirier, L. J. Abbott, N. A. Lynd, K. I. Winey, A. L. Frischknecht and T. M. Alam, *Macromolecules*, 2019, **52**, 857–876.
- 13 A. Kusoglu and A. Z. Weber, *Chem. Rev.*, 2017, **117**, 987–1104.
- 14 T. Nakagawa, K. Nakabayashi, T. Higashihara and M. Ueda, *J. Polym. Sci. A Polym. Chem.*, 2011, **49**, 2997–3003.
- 15 E. P. Jutemar and P. Jannasch, *J. Membr. Sci.*, 2010, **351**, 87–95.
- 16 O. Savard, T. J. Peckham, Y. Yang and S. Holdcroft, *Polymer*, 2008, **49**, 4949–4959.
- 17 A. Roy, H.-S. Lee and J. E. McGrath, *Polymer*, 2008, **49**, 5037–5044.
- 18 K. Nakabayashi, K. Matsumoto and M. Ueda, *J. Polym. Sci. A Polym. Chem.*, 2008, **46**, 3947–3957.
- 19 K. Nakabayashi, K. Matsumoto, T. Higashihara and M. Ueda, *J. Polym. Sci. A Polym. Chem.*, 2008, **46**, 7332–7341.
- 20 N. Asano, K. Miyatake and M. Watanabe, *J. Polym. Sci. A Polym. Chem.*, 2006, **44**, 2744–2748.
- 21 B. Bae, K. Miyatake and M. Watanabe, *Macromolecules*, 2010, **43**, 2684–2691.
- 22 N. Li, S. Y. Lee, Y.-L. Liu, Y. M. Lee and M. D. Guiver, *Energy Environ. Sci.*, 2012, **5**, 5346–5355.
- 23 N. Asano, M. Aoki, S. Suzuki, K. Miyatake, H. Uchida and M. Watanabe, *J. Am. Chem. Soc.*, 2006, **128**, 1762–1769.
- 24 M. Maalouf, C.-N. Sun, B. Pyle, M. Emery, G. M. Haugen, S. J. Hamrock and T. A. Zawodzinski, *Int. J. Hydrog. Energy*, 2014, **39**, 2795–2800.
- 25 K. Kidena, T. Ohkubo, N. Takimoto and A. Ohira, *Eur. Polym. J.*, 2010, **46**, 450–455.
- 26 A. Kusoglu, K. Vezzù, G. A. Hegde, G. Nawn, A. R. Motz, H. N. Sarode, G. M. Haugen, Y. Yang, S. Seifert, M. A. Yandrasits, S. Hamrock, C. M. Maupin, A. Z. Weber, V. Di Noto and A. M. Herring, *Chem. Mater.*, 2020, **32**, 38–59.

- 27 S. Shi, A. Z. Weber and A. Kusoglu, *J. Membr. Sci.*, 2016, **516**, 123–134.
- 28 N. Li, D. S. Hwang, S. Y. Lee, Y.-L. Liu, Y. M. Lee and M. D. Guiver, *Macromolecules*, 2011, **44**, 4901–4910.
- 29 X. Qiu, M. Ueda, H. Hu, Y. Sui, X. Zhang and L. Wang, *ACS Appl. Mater. Interfaces*, 2017, **9**, 33049–33058.
- 30 R. Jiang, H. R. Kunz and J. M. Fenton, *J. Power Sources*, 2005, **150**, 120–128.
- 31 C. Wang, S. Young Lee, D. Won Shin, N. Rae Kang, Y. M. Lee and M. D. Guiver, *J. Membr. Sci.*, 2013, **427**, 443–450.
- 32 A. Rohatgi, *WebPlotDigitizer*, <https://automeris.io>.
- 33 B. Bae, T. Yoda, K. Miyatake, H. Uchida and M. Watanabe, *Angew Chem Int Ed*, 2010, **49**, 317–320.
- 34 T. Ban, M. Guo, Y. Wang, Y. Zhang and X. Zhu, *J. Membr. Sci.*, 2023, **668**, 121255.
- 35 T. Higashihara, K. Matsumoto and M. Ueda, *Polymer*, 2009, **50**, 5341–5357.
- 36 C. Jin, X. Zhu, S. Zhang and S. Li, *Polymer*, 2018, **148**, 269–277.
- 37 B. Lafitte and P. Jannasch, *Adv Funct Materials*, 2007, **17**, 2823–2834.
- 38 S. Takamuku, E. A. Weiber and P. Jannasch, *ChemSusChem*, 2013, **6**, 308–319.
- 39 D. S. McLachlan, R. Rosenbaum, A. Albers, G. Eytan, N. Grammatica, G. Hurvits, J. Pickup and E. Zaken, *J. Phys.: Condens. Matter*, 1993, **5**, 4829–4842.
- 40 F. Vargas-Lara and J. F. Douglas, *Soft Matter*, 2015, **11**, 4888–4898.
- 41 G. S. Park, *Synthetic Membranes: Science, Engineering and Applications*, Springer Netherlands, Dordrecht, 1986, pp. 57–107.
- 42 B. Mecheri, V. Felice, Z. Zhang, A. D'Epifanio, S. Licoccia and A. C. Tavares, *J. Phys. Chem. C*, 2012, **116**, 20820–20829.
- 43 V. Detallante, D. Langevin, C. Chappey, M. Métayer, R. Mercier and M. Pinéri, *J. Membr. Sci.*, 2001, **190**, 227–241.
- 44 Y. Wu, M. Adamski, H.-F. Lee and S. Holdcroft, *J. Membr. Sci.*, 2020, **610**, 118276.
- 45 N. Zhao, D. Edwards, Z. Shi and S. Holdcroft, *EEL*, 2013, **2**, F22–F24.
- 46 Y. S. Kim, B. Einsla, M. Sankir, W. Harrison and B. S. Pivovar, *Polymer*, 2006, **47**, 4026–4035.
- 47 Y. Bai, M. S. Schaberg, S. J. Hamrock, Z. Tang, G. Goenaga, A. B. Papandrew and T. A. Zawodzinski, *Electrochimica Acta*, 2017, **242**, 307–314.
- 48 M. Adamski, N. Peressin and S. Holdcroft, *Mater. Adv.*, 2021, **2**, 4966–5005.
- 49 A. Z. Weber and J. Newman, *Chem. Rev.*, 2004, **104**, 4679–4726.
- 50 A. R. Crothers, R. M. Darling, A. Kusoglu, C. J. Radke and A. Z. Weber, *J. Electrochem. Soc.*, 2020, **167**, 013548.
- 51 A. R. Crothers, R. M. Darling, A. Kusoglu, C. J. Radke and A. Z. Weber, *J. Electrochem. Soc.*, 2020, **167**, 013547.
- 52 T. M. Alam, *J. Phys. Chem. A*, 2018, **122**, 3927–3938.
- 53 T. Munegumi, *World J. Chem. Educ.*, **1**, 12–16.
- 54 J. P. Guthrie, *Can. J. Chem.*, 1978, **56**, 2342–2354.
- 55 A. Trummal, L. Lipping, I. Kaljurand, I. A. Koppel and I. Leito, *J. Phys. Chem. A*, 2016, **120**, 3663–3669.
- 56 R. B. Nuernberg, *Ionics*, 2020, **26**, 2405–2412.
- 57 P. Grathwohl, *Diffusion in Natural Porous Media: Contaminant Transport, Sorption/Desorption and Dissolution Kinetics*, Springer US, Boston, MA, 1998, vol. 1.
- 58 S. Ochi, O. Kamishima, J. Mizusaki and J. Kawamura, *Solid State Ionics*, 2009, **180**, 580–584.
- 59 P. Knauth and M. L. Di Vona, *Front. Energy Res.*, 2014, **2**, 1–6.
- 60 P. Knauth, L. Pasquini, R. Narducci, E. Sgreccia, R.-A. Becerra-Arciniegas and M. Di Vona, *J. Membr. Sci.*, 2021, **617**, 118622.
- 61 C. De Grotthuss, *BBA*, 2006, **1757**, 871–875.
- 62 B. R. Cherry, C. H. Fujimoto, C. J. Cornelius and T. M. Alam, *Macromolecules*, 2005, **38**, 1201–1206.
- 63 L. He, C. J. Cornelius and D. Perahia, *Eur. Polym. J.*, 2014, **56**, 168–173.
- 64 C. Chen, Y.-L. S. Tse, G. E. Lindberg, C. Knight and G. A. Voth, *J. Am. Chem. Soc.*, 2016, **138**, 991–1000.
- 65 N. Agmon, *Chem. Phys. Lett.*, 1995, **244**, 456–462.
- 66 N. C. Osti, T. N. Etampawala, U. M. Shrestha, D. Aryal, M. Tyagi, S. O. Diallo, E. Mamontov, C. J. Cornelius and D. Perahia, *The Journal of Chemical Physics*, 2016, **145**, 224901.
- 67 S. Peighambaroust, S. Rowshanzamir and M. Amjadi, *Int. J. Hydrog. Energy*, 2010, **35**, 9349–9384.
- 68 A. K. Sahu, S. Pitchumani, P. Sridhar and A. K. Shukla, *Bull Mater Sci*, 2009, **32**, 285–294.
- 69 L.-Y. Zhu, Y.-C. Li, J. Liu, J. He, L.-Y. Wang and J.-D. Lei, *Pet. Sci.*, 2022, **19**, 1371–1381.
- 70 Z. Zuo, Y. Fu and A. Manthiram, *Polymers*, 2012, **4**, 1627–1644.
- 71 L. J. Abbott and A. L. Frischknecht, *Macromolecules*, 2017, **50**, 1184–1192.
- 72 S. Paddison, *Annu. Rev. Mater. Res.*, 2003, **33**, 289–319.
- 73 A. Barnett, J. Lu and V. Molinero, *J. Phys. Chem. C*, 2021, **125**, 27703–27713.
- 74 A. R. Crothers, A. Kusoglu, C. J. Radke and A. Z. Weber, *Langmuir*, 2022, **38**, 10362–10374.
- 75 J. Savage, Y.-L. S. Tse and G. A. Voth, *J. Phys. Chem. C*, 2014, **118**, 17436–17445.
- 76 P. Guan, J. Lei, X. Liu, K. Xu, S. Pei, H. Ding, Y. Zou, W. Feng, F. Liu and Y. Zhang, *Chem. Mater.*, 2022, **34**, 7845–7857.
- 77 M. K. Petersen and G. A. Voth, *J. Phys. Chem. B*, 2006, **110**, 18594–18600.
- 78 Z. Zhu, X. Luo and S. J. Paddison, *Chem. Rev.*, 2022, **122**, 10710–10745.
- 79 K.-D. Kreuer, S. J. Paddison, E. Spohr and M. Schuster, *Chem. Rev.*, 2004, **104**, 4637–4678.
- 80 A. Siu, J. Schmeisser and S. Holdcroft, *J. Phys. Chem. B*,

- 2006, **110**, 6072–6080.
- 81 M. Sahini and M. Sahimi, *Applications Of Percolation Theory*, CRC Press, 0th edn, 1994.
 - 82 S. Kirkpatrick, *Rev. Mod. Phys.*, 1973, **45**, 574–588.
 - 83 S. L. Zelinka, *WOOD FIBER SCI.*, 2008, **40**, 544–552.
 - 84 J. Kováčik, *Scripta Materialia*, 1998, **39**, 153–157.
 - 85 D. S. McLachlan, *J. Electroceram.*, 2000, **5**, 93–110.
 - 86 D. McLachlan, C. Chiteme, W. Heiss and J. Wu, *Physica B: Condensed Matter*, 2003, **338**, 261–265.
 - 87 Z. Li, J. Fu, X. Zhou, S. Gui, L. Wei, H. Yang, H. Li and X. Guo, *Adv. Sci.*, 2023, **10**, 2201718.
 - 88 M. Newville, T. Stensitzki, D. B. Allen and A. Ingargiola, *LM-FIT: Non-Linear Least-Square Minimization and Curve-Fitting for Python*, Zenodo, 2014.
 - 89 K. Levenberg, *Quart. Appl. Math.*, 1944, **2**, 164–168.
 - 90 D. W. Marquardt, *SIAM*, 1963, **11**, 431–441.
 - 91 S. B. Smedley, Y. Chang, C. Bae and M. A. Hickner, *Solid State Ion.*, 2015, **275**, 66–70.
 - 92 M. A. Barique, E. Tsuchida, A. Ohira and K. Tashiro, *ACS Omega*, 2018, **3**, 349–360.
 - 93 C. Luo, Q. Guo, C. Feng, Y. Wang, P. Ming and C. Zhang, *J. Electrochem. Soc.*, 2024, **171**, 034513.
 - 94 J. Peng, M. Tian, N. M. Cantillo and T. Zawodzinski, *Electrochimica Acta*, 2018, **282**, 544–554.
 - 95 I. Webman, J. Jortner and M. H. Cohen, *Phys. Rev. B*, 1976, **14**, 4737–4740.
 - 96 G. Gebel, *Polymer*, 2000, **41**, 5829–5838.
 - 97 Z. Zhang, L. Hu, R. Wang, S. Zhang, L. Fu, M. Li and Q. Xiao, *Polymers*, 2024, **16**, 545.
 - 98 W. Y. Hsu, J. R. Barkley and P. Meakin, *Macromolecules*, 1980, **13**, 198–200.
 - 99 X. Tongwen, Y. Weihua and H. Binglin, *Chem. Eng. Sci.*, 2001, **56**, 5343–5350.
 - 100 Y. A. Elabd, C. W. Walker and F. L. Beyer, *J. Membr. Sci.*, 2004, **231**, 181–188.
 - 101 Y. A. Elabd, E. Napadensky, J. M. Sloan, D. M. Crawford and C. W. Walker, *J. Membr. Sci.*, 2003, **217**, 227–242.
 - 102 S. J. Paddison, G. Bender, K.-D. Kreuer, N. Nicoloso and T. A. Z. Jr, *J. New Mater. Electrochem. Syst.*, 2000.
 - 103 K.-D. Kreuer and G. Portale, *Adv Funct Materials*, 2013, **23**, 5390–5397.
 - 104 L. Pisani, M. Valentini, D. Hofmann, L. Kuleshova and B. D’Aguanno, *Solid State Ionics*, 2008, **179**, 465–476.
 - 105 X. Luo, G. Lau, M. Tesfaye, C. R. Arthurs, I. Cordova, C. Wang, M. Yandrasits and A. Kusoglu, *J. Electrochem. Soc.*, 2021, **168**, 104517.
 - 106 M. A. Yandrasits, J. Condon, A. J. Steinbach, M. Novy and K. Patel, *J. Electrochem. Soc.*, 2024, **171**, 074504.
 - 107 Z. Zhu, N. M. Walsby, H. M. Colquhoun, D. Thompson and E. Petrucco, *FUEL CELLS*, 2009, **9**, 305–317.
 - 108 J. Miyake, R. Taki, T. Mochizuki, R. Shimizu, R. Akiyama, M. Uchida and K. Miyatake, *Sci. Adv.*, 2017, **3**, eaao0476.
 - 109 N. Peressin, M. Adamski, E. M. Schibli, E. Ye, B. J. Frisken and S. Holdcroft, *Macromolecules*, 2020, **53**, 3119–3138.
 - 110 S. A. Berlinger, P. J. Dudenas, A. Bird, X. Chen, G. Freychet, B. D. McCloskey, A. Kusoglu and A. Z. Weber, *ACS Appl. Polym. Mater.*, 2020, **2**, 5824–5834.
 - 111 R. Silva, M. De Francesco and A. Pozio, *Electrochimica Acta*, 2004, **49**, 3211–3219.
 - 112 P. J. Dudenas and A. Kusoglu, *Macromolecules*, 2019, **52**, 7779–7785.
 - 113 Novy, Melissa H. L., *PhD thesis*, Virginia Tech, Blacksburg, Virginia, 2022.
 - 114 S.-H. Shin, P. J. Nur, A. Kodir, D.-H. Kwak, H. Lee, D. Shin and B. Bae, *ACS Omega*, 2019, **4**, 19153–19163.
 - 115 C. Yin, Z. Wang, Y. Luo, J. Li, Y. Zhou, X. Zhang, H. Zhang, P. Fang and C. He, *J. Phys. Chem. Solids*, 2018, **120**, 71–78.
 - 116 J. N. Pratama, H. Song, H. Kim, H. Lee, D. Shin and B. Bae, *Polymers*, 2024, **16**, 1348.
 - 117 J.-D. Kim and L.-J. Ghil, *Int. J. Hydrog. Energy*, 2016, **41**, 11794–11800.
 - 118 S. He, Y. Lin, H. Ma, H. Jia, X. Liu and J. Lin, *Mater. Lett.*, 2016, **169**, 69–72.
 - 119 H. Mendil-Jakani, I. Zamanillo Lopez, P. M. Legrand, V. H. Mareau and L. Gonon, *Phys. Chem. Chem. Phys.*, 2014, **16**, 11243–11250.
 - 120 M. Adamski, T. J. G. Skalski, S. Xu, M. Killer, E. M. Schibli, B. J. Frisken and S. Holdcroft, *Polym. Chem.*, 2019, **10**, 1668–1685.
 - 121 M. A. Barique, L. Wu, N. Takimoto, K. Kidena and A. Ohira, *J. Phys. Chem. B*, 2009, **113**, 15921–15927.